Colloids and Surfaces B: Biointerfaces 253 (2025) 114736

Contents lists available at ScienceDirect

Colloids and Surfaces B: Biointerfaces

journal homepage: www.elsevier.com/locate/colsurfb

Novel hydrogel-based cancer-on-a-chip models for growth of 3D multi-cellular structures and investigation of early angiogenesis in pancreatic ductal adenocarcinoma

Karinna Georgiana Pele [a], Alejandro Calderón-Villalba [a], Hippolyte Amaveda [b], Mario Mora [b], Jack Zhang-Zhou [a], María Ángeles Pérez [a,c], José Manuel García-Aznar [a,c], Pilar Alamán-Díez [a], Elena García-Gareta [a,c,d,*]

[a] Multiscale in Mechanical & Biological Engineering Research Group, Aragon Institute of Engineering Research (I3A),School of Engineering & Architecture, University of Zaragoza, Zaragoza, Aragon 50018, Spain
[b] Instituto de Nanociencia y Materiales de Aragón (INMA), CSIC and University of Zaragoza, Zaragoza, Aragon 50018, Spain
[c] Aragon Institute for Health Research (IIS Aragon), Miguel Servet University Hospital, Zaragoza, Aragon 50009, Spain
[d] Division of Biomaterials & Tissue Engineering, UCL Eastman Dental Institute, University College London, London NW3 2QG, United Kingdom

ARTICLE INFO

Keywords:
Pancreatic ductal adenocarcinoma
Cancer-on-a-chip
Egg white
Gelatin
Angiogenesis

ABSTRACT

Cancer-on-a-chip models have enormous potential for the study of tumour development events. Here, we investigated hydrogels of egg white (EW) and gelatin for growth of 3D multi-cellular structures and investigation of early angiogenesis inside microfluidic devices. We focused on pancreatic ductal adenocarcinoma (PDAC), a devastating gastrointestinal malignancy. EW/gelatin hydrogels were stiffer and showed porous globular structures compared to the fibrous network of collagen I molecules. PANC-1 cells preferentially formed significantly larger spheroids in collagen I than in EW/gelatin hydrogels, whilst cell aggregates in the shape of grape-like clusters were significantly larger and more abundant in EW/gelatin. Cells inside the aggregates showed active cell unions, secreted matrix, and formed active unions with the surrounding EW/gelatin hydrogel. Early stages of PDAC were recreated by co-culture of two different microenvironments, one for PANC-1 and another one for fibroblasts, for investigating the secretion of soluble angiogenic factors, which depended on the role of each factor in the angiogenic and tumorigenic processes. Overall, cancer cell proliferation and establishment of a tumour vasculature were favoured. This study demonstrates the importance of the microenvironment in tumour cells behaviour as well as the complex interplay between the different cells present in PDAC to establish a tumoural vasculature.

1. Introduction

Tissue-engineered cancer models inside microfluidic platforms, i.e. cancer-on-a-chip, have become attractive and powerful tools in cancer research [1]. These miniaturized cancer models can mimic a particular stage of the tumour development [1] and need a hydrogel material that allows cell growth and function, preferably the formation of three-dimensional (3D) multi-cellular structures. In contrast with traditional two-dimensional (2D) culture systems, 3D multi-cellular structures such as aggregates and spheroids are able to mimic some characteristics of solid tumours with great precision (2): they show a hypoxic centre surrounded by a well-oxygenated outer layer of cells, they contain cells exposed in their surface as well as deeply buried inside, and both proliferating and non-proliferating cells are present [2]. Moreover, they mimic tumoural behaviour as they can faithfully replicate their physiological responses, gene expression, secretion of soluble mediators or drug resistance mechanisms [3]. All of this makes 3D multi-cellular structures a very appealing tool for their application in cancer research [4].

Hydrogels are the materials of choice for building cancer-on-a-chip models [5-8], as they mimic certain aspects of the extracellular matrix (ECM), such as viscoelasticity and a hydrated nature [9,10], and those

* Corresponding author at: Multiscale in Mechanical & Biological Engineering Research Group, Aragon Institute of Engineering Research (I3A),School of Engineering & Architecture, University of Zaragoza, Aragon, Zaragoza 50018, Spain.
E-mail address: garciage@unizar.es (E. García-Gareta).

https://doi.org/10.1016/j.colsurfb.2025.114736
Received 7 October 2024; Received in revised form 27 March 2025; Accepted 23 April 2025
Available online 30 April 2025

made of natural sources contain ECM components and cues, offering a highly biocompatible 3D environment for cell growth [10]. Chicken egg white (EW) is a native biomaterial with renowned biological, structural and physico-chemical characteristics [11]. Proteins are its principal component, imparting both its physical and biological properties [11]. Although historically underappreciated, in recent years an increasing amount of research is investigating EW's biological applications. This is because of its bioactivity in addition to its recognized antibacterial, wound healing, anti-inflammatory and cell growth properties [11]. Gelatin, derived from collagen through acid- or alkali-catalyzed hydrolysis, is a natural and biodegradable animal protein. Its biocompatibility and cell-adhesion properties make it a popular choice for biomedical applications [12,13]. Mixtures of EW and gelatin have been used in food chemistry research to study different properties such as its thickness and viscoelasticity depending on gelatin concentration, or the porosity of the hydrogels as a function of the amount of gelatin added to the mix [14, 15]. The feasibility of using mixed hydrogels of EW and gelatin for tissue engineering applications was studied by our group [16]. Our work showed the fabrication of 3D hydrogel scaffolds with pores, globular nano-topography and adjustable mechanical properties, as well as the use of miniature 3D hydrogels in microfluidic devices [16]. This provides a basis for their use in cancer-on-a-chip models for investigating tumour development phenomena. To the best of our knowledge, no studies have used these mixed EW/gelatin hydrogels in cancer-on-a-chip models. Although there are examples where EW was used to grow 3D multi-cellular structures, these studies used unprocessed EW and traditional culture dishes [17,18]. Our developed fabrication method ensures consistency of EW protein content and adds the cell adhesion properties of gelatin due to its plentiful RGD sequences [13,16]. Moreover, our work uses microfluidic devices for precise control of the microenvironment and culture conditions [16].

In this study we focused on pancreatic ductal adenocarcinoma (PDAC), which is a devastating gastrointestinal malignancy representing the third leading cause of death from cancer in the US [19]. It has an average 5-year survival rate moderately over 5 % due to its late-stage detection, aggressiveness, lack of effective systemic or immune therapies, and low disease prevalence [19-21]. The tumour microenvironment (TME) of PDAC consists of cancer cells surrounded by non-malignant stromal cells [22,23]. Fibroblasts, a major component in PDAC stroma, are referred to as cancer-associated-fibroblasts (CAFs). Initially arriving at the tumour site as normal fibroblasts, CAFs remain perpetually activated and do not revert to a normal phenotype or undergo apoptosis and elimination [22,24]. Tumours gradually develop a TME characterized by hypoxia, ischemia, acidosis and high interstitial fluid pressure. This environment releases numerous growth factors and cytokines, which stimulate angiogenesis and lymphangiogenesis to support the tumour's growth and metabolic demands [25,26]. Considering the significant role of angiogenesis in tumour growth and metastasis, the long-term survival of PDAC patients could be enhanced with the development of anti-angiogenic agents. However, contradictory results have been obtained, signalling the need for further research into the formation of a vascular network in PDAC [27].

The aim of this work was the development of hydrogel-based cancer-on-a-chip models for growth of 3D multi-cellular structures and investigation of early angiogenesis in PDAC. This work had two distinct parts. The first part encompassed PANC-1 3D multi-cellular structures growth in two prototypes of EW/gelatin hydrogels inside microfluidic devices. The second part involved the development of a cancer-on-a-chip model with two different microenvironments, i.e. one for PANC-1 3D multi-cellular structures in EW/gelatin hydrogel and one for normal fibroblasts inside a rich collagen I hydrogel, that mimicked an early PDAC development stage to study secretion of angiogenic factors and cytokines.

2. Materials and methods

2.1. Egg white/gelatin hydrogels

Chicken (*Gallus gallus domesticus*) eggs from a local supermarket were cracked open in Petri dishes. Avoiding the yolk and chalaza, the EW was transferred to Eppendorf tubes and lyophilized, obtaining a powder that was stored at 4 °C. Using the lyophilized EW powder and gelatin (Type B, from bovine skin, Merck, Spain), two colloidal solutions were prepared in distilled water (dH_2O): 5 % EW + 1 % gelatin and 5 % EW + 5 % gelatin. The pH of the hydrocolloids was adjusted to neutral (pH = 7.0 ± 0.5) to mimic physiological pH and prevent cytotoxicity. These solutions were then used for producing hydrogels by heating at 80 °C for 30 min followed by cooling at 4 °C overnight (Fig. 1A).

2.2. Collagen I hydrogels

Collagen hydrogels, with a final collagen concentration of 6 mg/ml, were prepared by diluting in an ice bath collagen type I solution (Rat Tail, stock 10.8 mg/ml, Corning, Spain), in Dulbecco's Modified Eagle Medium (DMEM, 4.5 g/L glucose, Thermo Fisher Scientific, Spain), 10x Dulbecco's phosphate buffered saline (DPBS) and 0.5 M NaOH (both from Sigma-Aldrich, Germany) to adjust the pH to 7.4–7.6 (Fig. 1A).

2.3. Scanning electron microcopy (SEM) of hydrogels

Freshly made hydrogels were dehydrated by lyophilization and coated with a 20 nm carbon film. An Inspect TM SEM F50 (FEI Company, Hillsboro, OR, USA) in an energy range between 0–30 keV was used to obtain SEM images of the hydrogels.

2.4. Rheology of hydrogels

Hydrogels were characterized using a stress-controlled rotational rheometer HAAKE Rheostress 1 (Thermo Fisher Scientific, Waltham, MA, USA). All samples were tested using a plate-plate configuration with a 35 mm diameter. 1 ml of each sample was deposited on the lower plate of the rheometer at 5 °C. Then, the upper plate descended until the gap between plates was the required by the sensor specifications (1 mm). A solvent trap was used to avoid sample dehydration. After allowing the sample to stabilize for 5 minutes at 5 °C, the oscillatory test was executed applying a fixed torque of 5 μNm at the frequency of 5 Hz, within the linear viscoelastic region (LVR) with a strain of amplitude 1 %. The storage G' and loss modulus G'', phase angle δ, and specific viscosity η* of each sample were recorded while the temperature gradually increased from 5 to 42 °C at a constant heating rate. The values of G', G'', δ and η* at 37 °C, the temperature at which the cells are cultured inside the hydrogels, was recorded.

2.5. Cell culture

The pancreatic cancer cell line PANC-1 from the American Type Culture Collection (ATCC, USA) and primary normal human dermal fibroblasts (HDFs, Lonza, Basel, Switzerland) were used for this work. These cells were cultured in Dulbecco's Modified Eagle Medium (DMEM, Gibco, Spain) with high glucose concentration and supplemented with 10 % fetal bovine serum (FBS, Life Technologies, Spain), 100 U/ml penicillin, 100 μg/ml streptomycin, and 2 mM L-glutamine (all from Lonza, Switzerland). Cultures were maintained in a humidified incubator set at 37 °C and 5 % CO_2.

2.6. Fabrication of microfluidic devices

For the fabrication of the microfluidic devices [7,16], we used a silicon wafer (Sandford University) with positive SU8 240-μm relief patterns with the desired geometry obtained by soft lithography. A

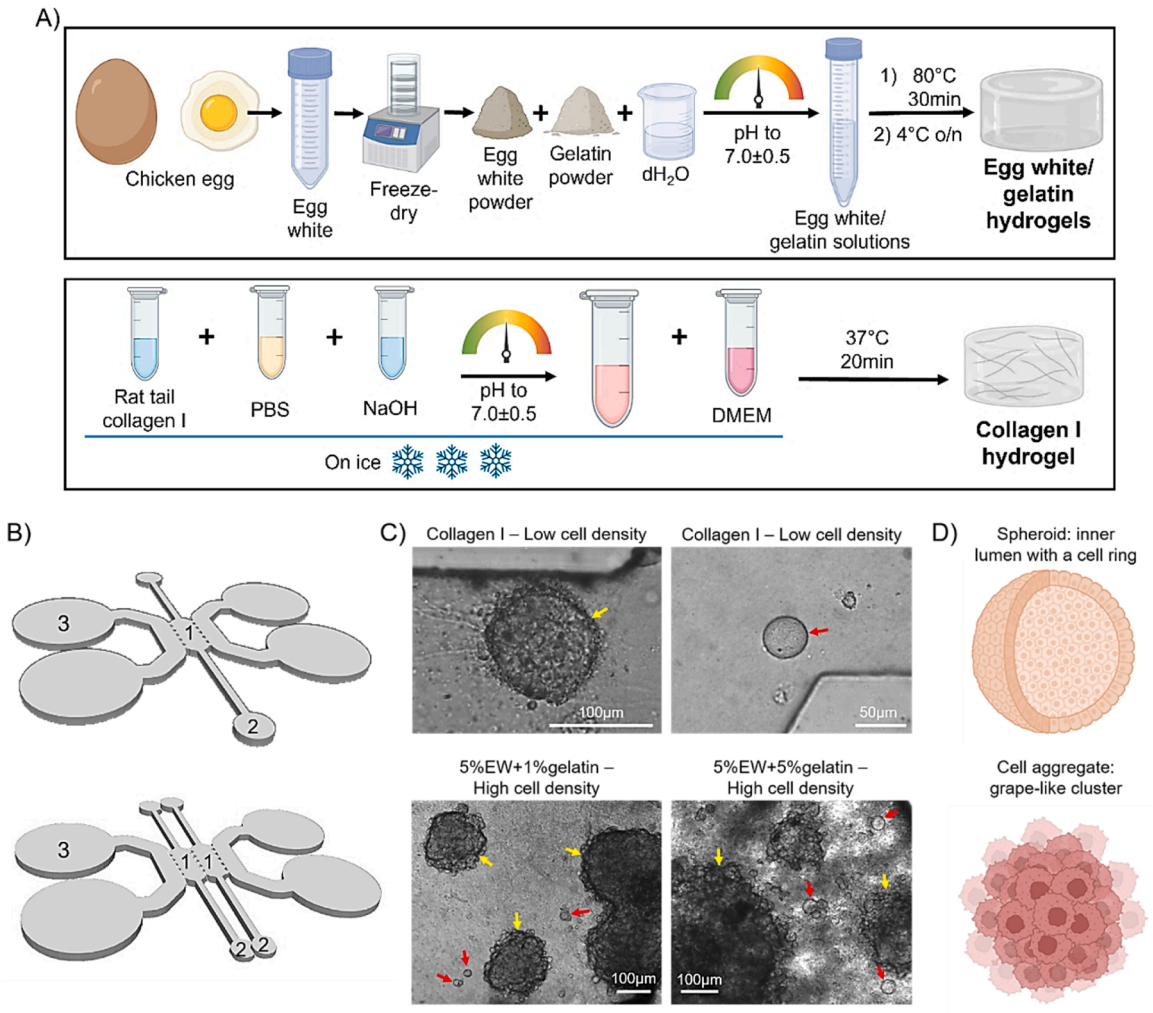

Fig. 1. A) Visual scheme of the fabrication protocols for producing the hydrogels of this study. Created with BioRender. **B)** Schematic of the microfluidic devices used in this study. Hydrogels and PANC-1 cells are introduced through the loading ports (2) into the central chambers of the devices (1). Culture medium is introduced through the reservoirs (3). **C)** Representative brightfield microscopy images of the two types of PANC-1 3D multi-cellular structures observed in this study inside microfluidic devices: spheroids (red arrows), with an inner lumen delimited by a cell ring, and cell aggregates (yellow arrows), with cells arranging in grape-like clusters. **D)** Schematic illustration showing the difference between spheroids and cell aggregates. Created with BioRender.

mixture of polydimethylsiloxane (PDMS, Sylargd 184, Dow Corning GmbH, Wiesbaden, Germany) was made at a 10:1 wt ratio of base to curing agent. The solution was poured into the SU8 wafer and degassed to remove air bubbles. The resulting layer was trimmed, perforated and autoclaved, then the PDMS devices were plasma-bonded to 35 mm glass-bottom petri dishes (Ibidi, Gräfelfing, Germany).

Two device geometries were used: one of them containing a single central chamber [7,16] and the other one containing two connected central chambers [28] (Fig. 1B). The one-chamber devices consisted of a central chamber (2.5 × 1.3 mm) containing an array of trapezoidal posts to cage the hydrogels and cells and two parallel side channels as medium reservoirs with a height of 300 µm. The devices with two chambers had the same dimensions but with two connected central chambers instead of one. In between the chambers, there was an array of trapezoidal posts to cage the different hydrogels and cells loaded into each chamber.

2.7. Polydopamine coating

Microfluidic devices to be loaded with collagen I were coated with polydopamine (PDA) to enhance collagen adhesion to the surface of the device [29]. A 0.5 mg/ml solution was prepared, by dissolving the required amount of dopamine hydrochloride (Sigma-Aldrich, Spain) in a 10 mM Tris-HCl buffer. The mixture was introduced through the small ports to cover the central chamber and incubated at room temperature for 1 h. The devices were then washed twice with dH_2O and dried at 60 °C overnight.

2.8. Cell seeding in microfluidic devices

The collagen I hydrogels at 6mg/ml were made as detailed in section 2.2 including the PANC-1 or HDFs suspension within the media. The collagen/cells solution was pipetted through the small ports and channels of the microfluidic device and left at 37 °C for 20 min to allow gelation. Cell culture media was then added through the reservoirs. Devices were then kept at 37 °C with 5 % CO_2.

As explained in section 2.1, two different EW/gelatin hydrogels were made. After gelation, approximately 4 µl of PANC-1 cell suspension were introduced through the small ports into the already formed hydrogels, then microfluidic devices were kept at 37 °C with 5 % CO_2 for 20 minutes. Finally, DMEM was added through medium channels and the devices kept at 37 °C with 5 % CO_2.

In the one-chamber devices, PANC-1 cells were seeded at two different densities, i.e. 2500 cells/device and 12500 cells/device; HDFs were seeded at 1000 cells/device. In the two-chamber devices, HDFs were seeded at 1000 cells/device whilst PANC-1 cells were seeded at

5000 cells/device.

2.9. Brightfield microscopy and quantification of 3D multi-cellular structures

Multi-cellular structures formation and growth in microfluidic devices (N = 3 per condition) was observed and photographed by brightfield microscopy (DM IL LED, Leica) over 14 days of culture. Multicellular structures were measured and characterized using the digital image processing software ImageJ (1.54 h, Java 13.0.6 64-bit, National Institutes of Health, USA). The silhouette of the cellular structures was manually cut out using tools in the software and data of their areas (μm^2) were obtained. The difference between what we categorized as spheroid or cell aggregate was morphological (Fig. 1C,D): spheroids had an inner lumen well delimited by a cell ring, while cell aggregates consist of several cells grouped together in the form of grape-like clusters. A total of 15 brightfield microscopy images were analyzed per group (5 images per device). All the structures present in the images were quantified. Data was plotted into violin plots using GraphPad software (GraphPad Prism 8.0.1 for Windows, Boston, Massachusetts, USA,). In the literature, the average diameter of PANC-1 tumour cells has been found to be up to 22.5 (± 3.8) μm [30], so the data was cut off at 380 μm^2, as structures smaller than this area were considered to be single cells.

2.10. Immunostaining and fluorescence microscopy

Microfluidic devices were fixed with 4 % paraformaldehyde (PFA) for 20 minutes, washed three times with PBS, sealed with parafilm, and kept at 4 °C. PBS was removed from the medium channels and replaced with a 0.1 % Triton X-100 solution in PBS, used to permeabilize the cell membrane, and left on a shaker for 15 minutes at room temperature. The solution was removed, and devices washed three times with PBS. Then, 5 % BSA in PBS was added through the reservoirs, and the devices placed on a shaker at 4 °C overnight. The next day, the staining solution was prepared within 0.5 % bovine serum albumin (BSA), diluting DAPI (1:1000) and phalloidin (1:100) and samples were dyed for 2 hours. Finally, after rinsing samples in PBS, the devices could be imaged or stored at 4 °C well covered in aluminum foil until observed. To avoid stain photobleaching, experiments were conducted with minimum light conditions. Stained samples were observed using a fluorescence microscope (Zeiss Axio Observer, Germany) in the corresponding emission range of each dye.

2.11. Dual-beam focused ion beam scanning electron microscopy (FIB-SEM) of microfluidic devices

A critical point drying (Leica EM CPD300) procedure was carried out in the one-chamber microfluidic devices containing EW/gelatin hydrogels. Before examination, these samples were also coated with a carbon film. A Dual-Beam Nova Nanolab 200 was used to acquire the secondary electron images. Initially, platinum was deposited by electron irradiation (FEBID) to protect the surface of the area to be analyzed from further damage, on which platinum was also deposited by ion irradiation (FIBID). This was followed by coarse milling by regular cross-sectioning using a current of 0.3 nA, after which different cleanings were performed by reducing the irradiation current to 50 pA.

2.12. Secretion of exogenous angiogenic cytokines and growth factors

Secretion of tumour necrosis factor alpha (TNFα), insulin-like growth factor 1 (IFG-1), vascular endothelial growth factor (VEGF), interleukin 6 (IL-6), fibroblast growth factor b (FGFb), transforming growth factor beta (TGFβ), epidermal growth factor (EGF) and leptin was profiled by ELISA (EA-1011, Signosis Inc, Sunnyvale, CA, USA). On day 3 after seeding, medium was collected (N = 4 per condition) and frozen at −80 °C. After thawing, supernatants were pipetted into coated wells (10 μL/well) and incubated for 1 h at room temperature with gentle shaking. Wells were washed 3 times with 200 μL wash buffer, 100 μL diluted biotin-labelled antibody mixture was added per well and incubated as before. After repeating the washing step, 100 μL of diluted streptavidin-HRP conjugate was added per well and incubated for 45 min at room temperature with gentle shaking. After washing, 100 μL of substrate was added per well and incubated for 30 min at room temperature. Finally, stop solution was added (50 μL/well). Absorbance at 450 nm was measured using a microplate reader (Synergy LX, BioTek with Gen5 3.10 software).

2.13. Data and statistical analysis

Data and statistical analysis were performed with GraphPad software (GraphPad Prism 8.0.1 for Windows, Boston, Massachusetts, USA). A non-parametric Mann-Whitney test was used to compare groups. A p value below 0.05 was considered a significant result.

3. Results

3.1. Characterization of egg white/gelatin and collagen I hydrogels

Macroscopic appearance of the hydrogels showed a difference in colour (Fig. 2A). Collagen I hydrogels were orange, because of the presence of phenol red, which is used as pH indicator during the fabrication process. The white appearance of the EW/gelatin hydrogels is due to the natural colour of gellified EW [11]. There were no observable macroscopic differences between the two EW/gelatin hydrogels. Interestingly, whilst collagen I hydrogels were transparent, the EW/gelatin ones had a degree of opacity. This could have implications for microscopy of cell cultures using these hydrogels.

In terms of microarchitecture (Fig. 2B), SEM images showed that the collagen I hydrogel was a complex mesh of nanofibers that formed a 3D porous microstructure with a range of pore sizes that included nano and micropores. On the other hand, SEM images of 5 % EW + 1 % gelatin showed a continuous dense mesh of globular proteins that coagulate and aggregate to form globular structures ranging from nano to micro sizes. The resulting hydrogel matrix was porous with nano and micropores. 5 % EW + 5 % gelatin SEM images showed continuous compact gels due to the high protein concentration, with a structure of aggregated globular proteins. Micropores were observed. Moreover, this hydrogel had a nanotextured surface.

Rheology results (Fig. 2C) showed that as the protein concentration of the EW/gelatin hydrogels increased, so did their elasticity, seen in an increment of the G′or elastic modulus when comparing the EW/gelatin gels [31], with G' higher than G'' in all cases. Although collagen I and 5 % EW + 1 % gelatin, which have the same amount of protein, did not show a significant difference when compared, a trend was seen towards 5 % EW + 1 % gelatin hydrogels being more elastic than collagen ones. A similar behaviour was noticed for the viscosity, which increased in the gel with higher protein concentration, showing a significant difference when comparing collagen I and 5 % EW + 1 % gelatin hydrogels with the 5 % EW + 5 % gelatin one. On the other hand, the phase angle δ decreased from collagen I to 5 % EW + 1 % gelatin and to 5 % EW + 5 % gelatin.

3.2. Growth of PANC-1 3D multi-cellular structures in hydrogels: brightfield microscopy and quantification of size and number

Both low cell density (2500 cells/device) and high cell density (12500 cells/device) cultures were established inside one-chamber microfluidic devices loaded with the three hydrogels used in this study: collagen I used as control, 5 % EW + 1 % gelatin and 5 % EW + 5 % gelatin (Figs. 3 and 4). Although brightfield microscopy was slightly more difficult on the EW/gelatin hydrogels, especially at low cell density, cells and multi-cellular structures were easily observed

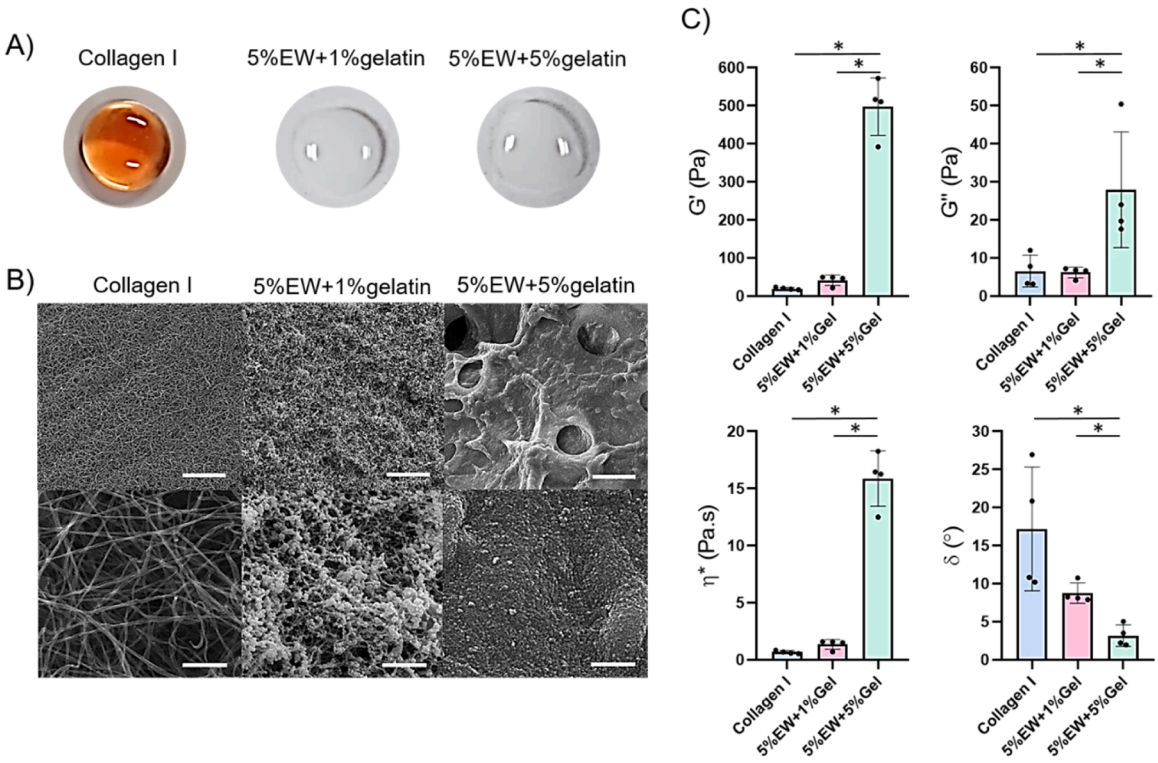

Fig. 2. A) Representative macroscopic images of approximately 5 mm diameter hydrogels. **B)** SEM images of hydrogels. Scale bar for images at the top is 10 μm and for images at the bottom is 1 μm. **C)** Rheology results for the hydrogels showing the storage modulus G', loss modulus G'', specific viscosity η* , and phase angle δ (Gel=gelatin). Graphs show mean ± standard deviation of N = 4 (individual data points shown).

(Figs. 3 and 4). Visualization on the 5 % EW + 5 % gelatin loaded devices was the most difficult due to the high protein content of this hydrogel. Over 14 days of culture, two distinct multi-cellular structures were formed: on the one hand spheroids, with an inner lumen well delimited by a cell ring, and on the other hand, cell aggregates with cells grouped together in the form of grape-like clusters (Fig. 1C). For the high cell density cultures, large 3D multi-cellular structures were observed in the three hydrogels of this study (Fig. 4). An important observation was that the collagen I hydrogel could not withstand the forces created by these large multi-cellular structures and eventually collapsed. Early signs of collagen I hydrogel displacement were seen on day 4 of culture. On the other hand, the EW/gelatin hydrogels remained in place for the duration of the experiment. In the low cell density cultures (Fig. 3) the collagen I hydrogels did not collapse as fewer cells were present.

Quantification of the 3D multi-cellular structures observed in the hydrogels showed that spheroids are preferentially formed at low cell density in the three hydrogels and specially in collagen I compared with both EW/gelatin hydrogels: for collagen I low cell density cultures, no cell aggregates were seen by the end of the culture, whilst the percentage of cell aggregates grew over time in the EW/gelatin cultures (Fig. 5A). The percentage of cell aggregates was larger in the high cell density cultures for the three hydrogels, and on day 14 of culture cell aggregates were more abundant than spheroids for the 5 % EW + 1 % gelatin hydrogel (Fig. 5A). In terms of size of the multi-cellular structures (Fig. 5B), the spheroids formed in collagen I were significantly larger than those formed in the EW/gelatin hydrogels. On the other hand, cell aggregates were significantly larger in the EW/gelatin hydrogels especially at low cell density.

3.3. Morphological characterization of PANC-1 3D multi-cellular structures in EW/gelatin hydrogels: fluorescence and dual-beam FIB-SEM microscopies

For further morphological characterization of the cell aggregates observed in the EW/gelatin hydrogels, fluorescence microscopy of DAPI/phalloidin stained cultures was used to make observations of the periphery as well as the core of the structures, whilst dual-beam FIB-SEM was used for close observation of the aggregates arrangement as well as their interaction with the surrounding hydrogel.

Fluorescence microscopy showed that the cell aggregates formed in EW/gelatin hydrogels had a compact nature (Fig. 6). For the larger aggregates (yellow arrow in Fig. 6), fewer and less compacted cells were seen at the core of the structures, probably due to limitations in oxygen and nutrients, which would be more available on the periphery of the aggregate [32], where a thick layer of cells was seen (up to 154 μm in thickness according to our images). The smaller aggregates (red arrow in Fig. 6) showed cells throughout the structure, suggesting an earlier degree of development compared with the larger aggregates.

Characterization using dual-beam FIB-SEM (Fig. 7) provided a close look at the aggregates, which indeed resembled grape-like clusters (Fig. 7A-C). The individual cells comprising the aggregates could be discerned and numerous microvilli were seen on their surface (Fig. 7A-C). Cross-sectioning of the aggregates showed that the cells formed active unions between them inside the multi-cellular structures (Fig. 7D). We could also see newly secreted matrix in the form of fibres (Fig. 7D,E, Fig. S1). Finally, we could also see active unions formed between cells and the hydrogel (Fig. 7F). We also looked at how the morphology of the EW/gelatin hydrogel changes after 14 days of incubation in culture media at 37 °C to be able to better understand the dual-beam FIB-SEM images (Fig. S1). The morphology of EW/gelatin hydrogels was modified, both showing globular structures with a denser appearance and a porous surface with both nano and micropores (Fig. S1). As mentioned, we saw the cells interacting with these globular structures of the EW/gelatin hydrogels (Fig. 7F).

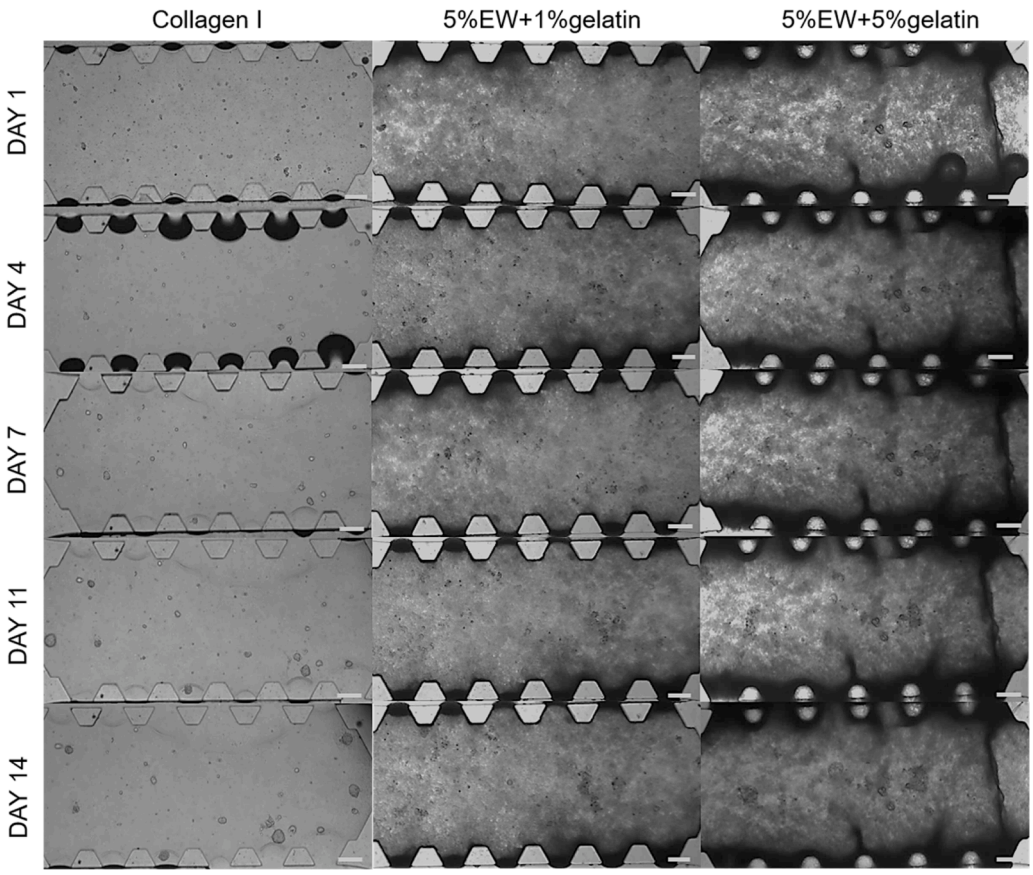

Fig. 3. Brightfield microscopy images of PANC-1 3D multi-cellular structures growth in hydrogels loaded inside one-chamber microfluidic devices: low cell density cultures. Images show the central chamber of the microfluidic device. Scale bar = 175 μm.

3.4. Cancer-on-a-chip hydrogel-based model with two different microenvironments that mimic an early stage of PDAC development: secretion of exogenous angiogenic cytokines and growth factors

For the second part of this study, two-chamber microfluidic devices capable of harbouring two different 3D microenvironments were used to seed HDFs and PANC-1 cells, in order to mimic early stages of PDAC where HDFs are arriving to the tumour site and have not yet differentiated to CAFs [33]. Therefore, we used a 5:1 PANC-1:HDFs ratio. One-chamber chips with either HDFs in collagen I or PANC-1 in 5 % EW + 1 % gelatin hydrogels were used as controls (Fig. 8A). We chose the 5 % EW + 1 % gelatin hydrogel over the more concentrated one due to easier microscopic observation.

As observed in the control chips, HDFs grew and proliferated as individual cells in collagen I hydrogels, where their characteristic elongated morphology could be seen at higher magnifications (Fig. 8B, top panel). On the other hand, PANC-1 cells grew and grouped forming 3D multi-cellular structures in the 5 % EW + 1 % gelatin hydrogels as already described (Fig. 8B, middle panel). In the two-chamber chips, two distinct microenvironments were observed, one with HDFs in collagen I and one with PANC-1 in 5 % EW + 1 % gelatin (Fig. 8B bottom panel, C). After one day of growth, PANC-1 cells began to group forming cell aggregates, visible on day 3 of culture (Fig. 8B,C).

Once the model with two different microenvironments was established, we investigated the secretion of exogenous angiogenic cytokines and growth factors by ELISA. Specifically, we looked at TNFα, IGF-1, VEGF, IL-6, FGFb, TGFβ, EGF and leptin [34]. Results showed that the secretion of the studied factors was not synergistic in the co-cultures (Fig. 9). It was observed that the secretion of some factors, like leptin, VEGF, FGFb and IGF-1 was favoured in the PANC-1 cultures and also in the co-cultures (Fig. 9A). Other factors like TGFβ, EGF and IL-6 had a slightly higher secretion in HDFs than in the co-culture (Fig. 9B). As for the secretion of TNFα, it was observed that the amount of this factor secreted in the PANC-1 cultures was significantly lower than IGF-1, VEGF, FGFb, TGFβ and leptin (Fig. 9A). However, in the co-cultures it was not significantly lower compared with the rest of the factors (Fig. 9A).

4. Discussion

Egg white and gelatin mixtures have been mainly investigated in the food chemistry sector due to the interesting features that appear when they are mixed together [14,15]. Limited studies in the biomedical field have combined EW with different materials for various applications [35-38], a few of which include the study of angiogenesis and cancer events [39,40]. Our group carried out a previous study on the feasibly of using EW and gelatin hydrogels for tissue engineering purposes, showing that they could be utilised in conjunction with microfluidic platforms to create 3D microenvironments for cell culture [16]. To the best of our knowledge, no studies have used these mixed EW/gelatin hydrogels in cancer-on-a-chip models. Therefore, we wanted to investigate EW/gelatin hydrogels for the growth of 3D multi-cellular PDAC tumour structures inside microfluidic platforms. We used collagen I hydrogels for comparison since they are widely used in the growth of 3D multi-cellular structures [29,41,7]. Collagen I hydrogels were also used for creating a biomimetic microenvironment for normal fibroblasts as these cells are the main responsible for secreting collagen I and forming structural ECMs rich in this protein [42]. Apart from collagen I, other hydrogels used in cancer-on-a-chip models include Matrigel [43], ECM hydrogels via tissue decellularization [44], methacryloyl platelet lysate [45], or PEGDA (polyethylene glycol diacrylate) [46]. However, these materials present disadvantages. For instance, Matrigel is well known

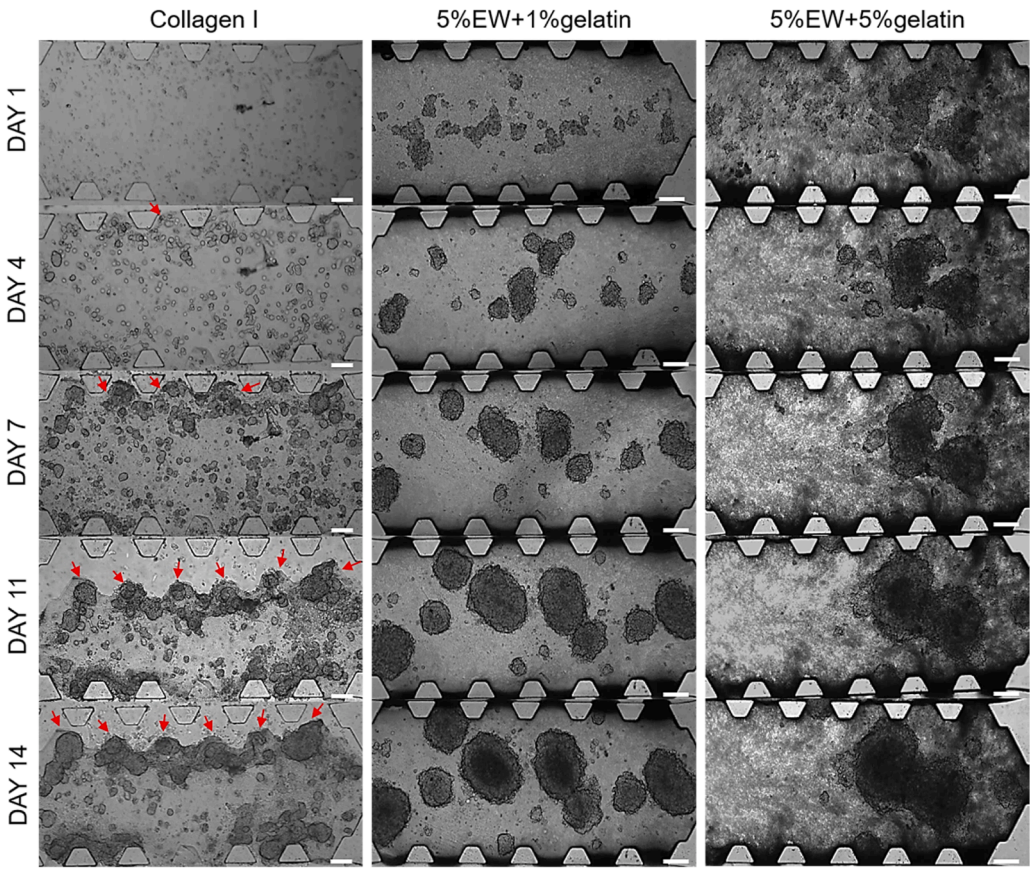

Fig. 4. Brightfield microscopy images of PANC-1 3D multi-cellular structures growth in hydrogels loaded inside one-chamber microfluidic devices: high cell density cultures. Images show the central chamber of the microfluidic device. Red arrows show displacement of the collagen I hydrogel. Scale bar = 175 μm.

for its batch-to-batch variation and ill-defined composition leading to lack of experimental reproducibility [47]. Collagen I also presents batch-to-batch variation and the microfluidic devices need to be coated with an adhesive component to preserve the hydrogel's mechanical integrity during culture [29]. Synthetic materials like PEGDA offer mechanical integrity but lack the molecular cues present in the ECM of tissues, resulting in reduced biocompatibility [48]. Finally, hydrogels like those derived from human tissue necessitate extensive and long processing, whilst availability of origin tissues is limited and is often subject to ethical regulation [49]. Based on the results from this paper, clear advantages of our proposed EW/gelatin hydrogel emerge, like easy availability, absence of ethical issues, cost-effectiveness, ease of fabrication and processing, reproducibility of results, presence of molecular cues found in the ECM of tissues, mechanical integrity, and effective growth of multi-cellular tumour structures.

The first step was the fabrication and characterization of the hydrogels. EW typically begins to coagulate or gel above 60 °C, with temperatures above 70 °C needed to achieve complete coagulation [50]. In this process, gelatin is trapped in the polymeric network of EW proteins that results from the formation of a gel. Gelatin denatures at around 40 °C [51], but a first stage thermal degradation of gelatin is not seen until 290 °C, with a second stage occurring at 420 °C [52]. Gelatin is partially denatured collagen, thereby unveiling the RGD sequences that are hidden in the collagen molecule [13,53]. By further denaturing the gelatin, more RGD sequences may become available. Finally, we cooled the gels at 4 °C to gellify the remaining gelatin that would be adsorbed onto the main EW network [12]. Following this sequential temperature process, mixed hydrogels of EW and gelatin were rendered. Collagen I gels are produced by controlling the pH of the collagen I solution, which gels around physiological pH. The gelation kinetic of collagen I is dependent on temperature, with higher temperatures accelerating the process [54]. The SEM results can be correlated with the molecular structure of the collagen and EW proteins. Whilst collagen is a polymeric fibrous protein, the proteins in EW have a globular morphology, which is kept when they aggregate [11,16,54]. Rheology results showed that as the protein concentration of the EW/gelatin hydrogels increased, so did their elasticity and viscosity, whilst the phase angle decreased, which means that gels have a more solid nature as their protein concentration increases. Therefore, our EW/gelatin hydrogels, specially the most concentrated one, are stiffer than collagen I hydrogel. Due to this rheological as well as the morphological differences seen, a different cellular behaviour would be expected on the different hydrogels.

Over the culture period, we observed the formation of two distinct multi-cellular structures as previously defined. Importantly, whilst the collagen I hydrogel could not withstand the forces created by the large multi-cellular structures of the high cell seeding density cultures, the EW/gelatin hydrogels remained in place for the duration of the experiment. These observations indicate that the EW/gelatin hydrogels may be an interesting tool for growing large multi-cellular structures of tumour cells that exert significant forces on the surrounding hydrogel, like PANC-1 cells. Our microscopy and quantification results suggest that the environment influences the morphological growth of 3D multi-cellular tumour structures, and are in agreement with previous studies were larger 3D multicellular structures of tumour cells were reported in stiffer gels [7,55]. The mechanical cues derived from stiffer microenvironments are sensed by tumour cells, thereby initiating an intracellular response that activates signalling pathways that culminate in increased cellular proliferation [56]. Particularly, sustained activation of the transcriptional regulators YAP/TAZ as a consequence of sensing a stiffer environment promotes tumour cell proliferation in numerous cancers including PDAC [57]. Nevertheless, further research is needed to

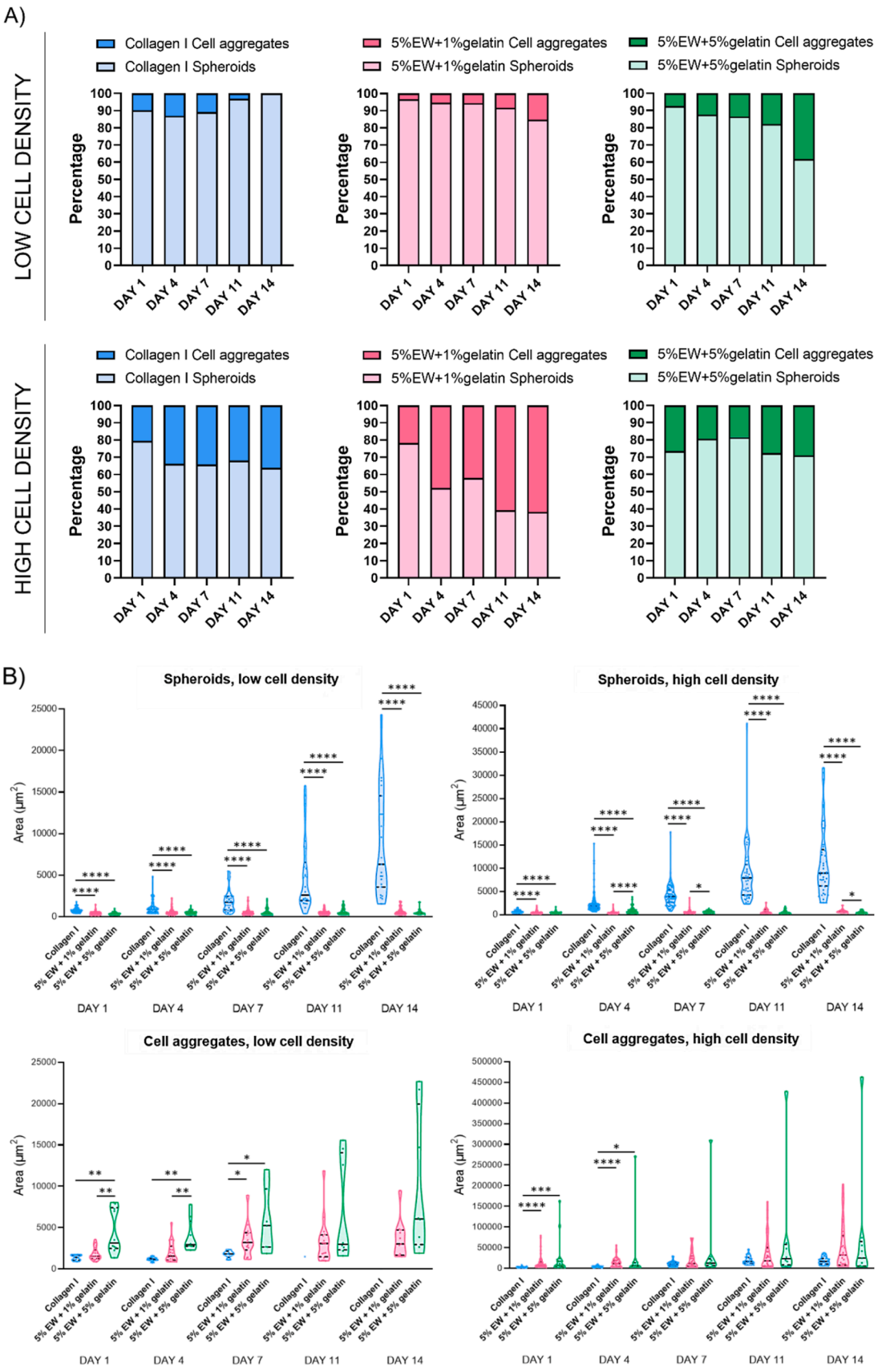

Fig. 5. Quantification of PANC-1 3D multi-cellular structures growth in hydrogels loaded inside one-chamber microfluidic devices. **A)** Percentage of spheroids and cell aggregates. **B)** Size of spheroids and cell aggregates. Violin plots show median, interquartile range and individual data points. *p < 0.05, * *p < 0.005, * **p < 0.0005, * ** *p < 0.0001.

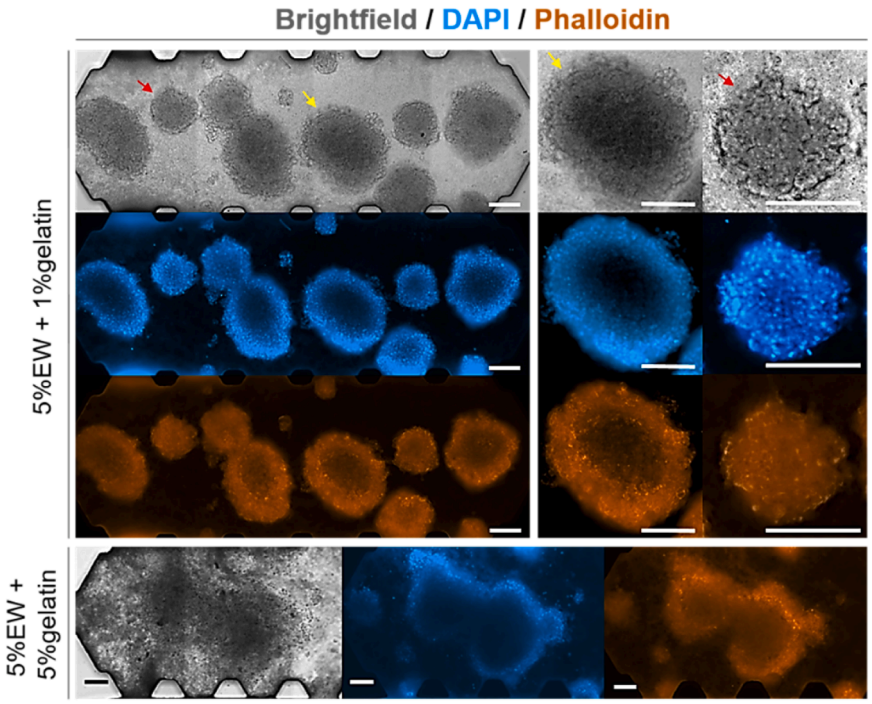

Fig. 6. Representative fluorescence microscopy images of cell aggregates formed in EW/gelatin hydrogels inside microfluidic devices after 14 days of culture, where the blue fluorescence is due to DAPI-stained dsDNA in the cells nuclei and the orange fluorescence is due to phalloidin-stained actin filaments in the cytoskeleton of cells. For the 5 %EW + 1 %gelatin panel, the images of individual aggregates on the right correspond to aggregates found in the main image of the whole central chamber of the microfluidic device (pointed at by red and yellow arrows). Scale bar = 175 μm.

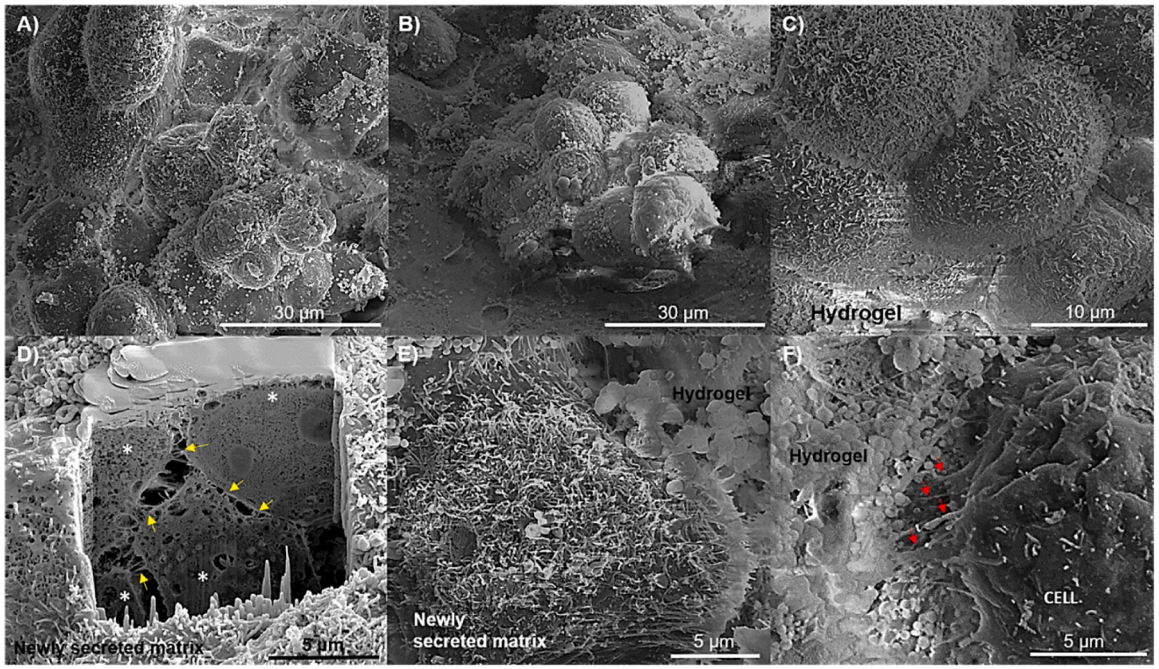

Fig. 7. Representative dual-beam FIB-SEM images of cell aggregates formed in EW/gelatin hydrogels inside microfluidic devices after 14 days of culture. **A, B, C)** partial views of cell aggregates where individual cells are discernible. **D)** Cross-section of an aggregate where 4 cells (*) can be seen. Yellow arrows point at unions between cells. **E)** Cell and newly secreted matrix. **F)** Active unions between cells and the surrounding hydrogel (red arrows).

accurately discern the mechanisms behind the formation of the different structures seen in this study. Whilst the cell spheroids observed here have been extensively described in the literature [2,3], the cell aggregates resembling grape-like clusters have been less frequently mentioned. An example is the work by Dayton and colleagues who observed the formation of grape-like clusters in patient-derived tumour organoids of neuroendocrine neoplasms [58]. These results prompted us to carry out further morphological characterization of the cell aggregates formed in EW/gelatin hydrogels by fluorescence and dual-beam FIB-SEM microscopies.

Fluorescence microscopy showed the compact nature of the cell aggregates formed in EW/gelatin hydrogels, with larger aggregates

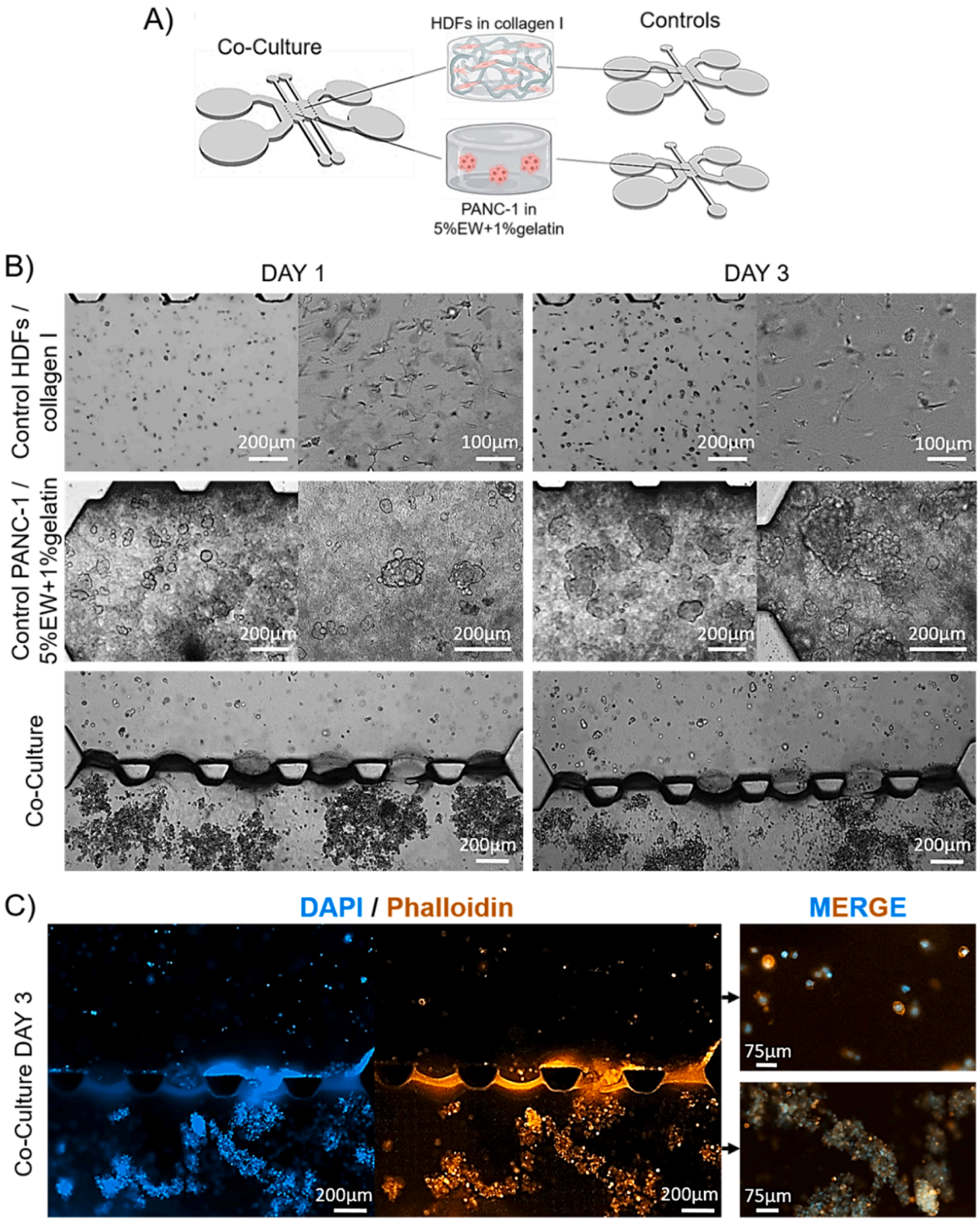

Fig. 8. A) Visual schematic of the experiment. **B)** Representative brightfield microscopy images of control cultures and co-cultures on days 1 and 3 of culture. **C)** Representative fluorescence microscopy images of co-cultures in two-chamber microfluidic devices on day 3 where the blue fluorescence is due to DAPI-stained dsDNA in the cells nuclei and the orange fluorescence is due to phalloidin-stained actin filaments in the cytoskeleton of cells. For both microenvironments, cells can be seen at different z-planes.

displaying fewer and less compacted cells at the core of the structures, and smaller aggregates showing cells throughout the structure, suggesting an earlier degree of development. Further work should look into the differences in metabolism between cells at different locations of the aggregates. Also, it would be interesting to examine whether the core of the aggregates has a hypoxic and acidic nature, as found in the TME of solid tumours like PDAC [59], which would make these structures highly analogue to in vivo tumours. Hypoxia in solid tumours like PDAC is recognized as a driving force of angiogenesis due to the necessity of cells present in the TME for oxygen and nutrients [59]. It has been described that with tumour diameters of less than 1 mm, there is no vessel formation, and cells obtain nutrients through permeation. In larger tumours, cells obtain nutrients through vessel formation. If this process of angiogenesis fails, tumour size is restricted to 2–3mm diameter due to lack of oxygen and nutrients for growth and development [59]. Moreover, acidosis in the TME is a consequence of hypoxia, having

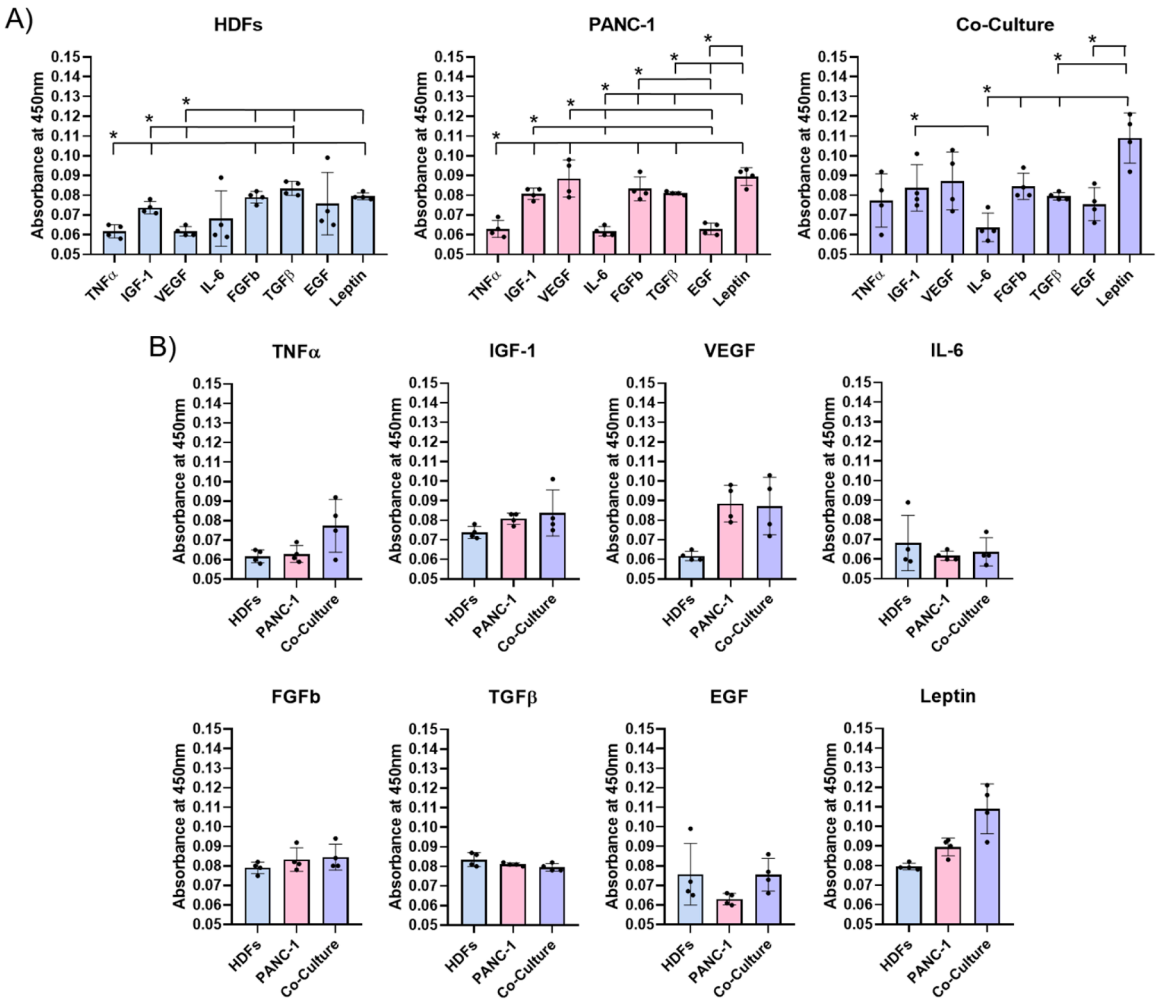

Fig. 9. A) Profile of angiogenic factors secretion for the individual control cultures and co-culture. **B)** Comparison of individual angiogenic factors across the different cultures. Graphs show mean ± standard deviation and the individual data points. *p<0.05.

significant implications in cancer cells metabolism [59]. Therefore, hypoxia and acidosis would be desirable features in 3D multi-cellular structures of PANC-1 cells in order to highly mimic the in vivo TME.

Dual-beam FIB-SEM morphological characterization showed extraordinary detail of the aggregates morphology and organization, the union between cells inside the aggregates, matrix secretion, and interaction of the cells with the surrounding environment. This minute morphological characterization is distinctive of the work presented here, as investigations concerning growth of 3D multi-cellular structures normally lack this level of detail. Furthermore, we identified new areas for further work, like investigation of the nature of the unions and the families of proteins that facilitate them, and identification of the composition of the newly secreted fibrous matrix.

The second part of this study entailed the use of two-chamber microfluidic devices capable of harbouring two different 3D microenvironments for HDFs and PANC-1 cells, to mimic early stages of PDAC where HDFs are arriving to the tumour site and have not yet differentiated to CAFs [35]. Once the model was established, we investigated the secretion of exogenous angiogenic cytokines and growth factors by ELISA. The activation of angiogenesis is governed by a large number of pro- and anti-angiogenic factors, and the balance between these factors is called the "angiogenic switch", which is a discrete step occurring at any stage of tumour progression depending on the nature and microenvironment of the tumour [60]. We looked at the classical angiogenic factors TNFα, IGF-1, VEGF, IL-6, FGFb, TGFβ, EGF and leptin [34]. TNFα has a role of suppression of tumour proliferation and induction of tumour regression [61]. However, Adjuto-Saccone and colleagues showed that TNF-α induces endothelial-mesenchymal transition of human endothelial cells thereby promoting the stromal development of PDAC [62]. Inhibition of apoptosis and stimulation of cell proliferation, thus promoting cancer development, has been shown for IGF-1 [63]. Similarly, FGFb initiates and promotes tumorigenesis, stimulating tumour cell proliferation and invasion [64]. Leptin is also linked to PDAC growth, metastasis, cancer cells proliferation, migration and invasion [65]. It also has effects on cancer stromal cells, enhancing angiogenesis and inflammatory processes to support tumour growth [66]. VEGF is a key mediator of angiogenesis. Its production results in the "angiogenic switch" with the formation of new vasculature around the tumour [67]. In PDAC patients, high levels of VEGF are associated with metastasis and poor prognosis [68]. In early stages of PDAC, TGFβ has tumour suppressive effects, with the inhibition of cell cycle progression and promotion of apoptosis. However, in late stages of PDAC it has tumour promoting effects, with the promotion of tumour invasiveness and metastasis [69,70]. IL-6 is part of the acquired immune response, stimulation of antibody production and effector T-cell development [71]. When its pathway is deregulated, it promotes proliferation, migration and adhesion among tumours including PDAC [72,73]. Finally, EGF has the physiological role of regulation of epithelial tissue development and homeostasis. In pathological conditions, EGF participates in tumorigenesis, pathogenesis and progression of different carcinoma types like PDAC [74].

Our results showed that the secretion of factors like leptin, VEGF,

FGFb and IGF-1 was favoured in the PANC-1 cultures and also in the co-cultures. VEGF is key in activating the "angiogenic switch" (60), while leptin plays an important role in tumour growth and metastasis [66]. On the other hand, IGF-1 and FGFb play important roles in cellular proliferation, invasiveness and tumorigenesis [63,64]. This would explain the observed overexpression of these factors in cultures where cancer cells are present. Other factors, i.e. TGFβ, EGF and IL-6, had a slightly higher secretion in HDFs than in the co-culture. In physiological conditions, EGF regulates epithelial tissue development [74] and IL-6 is part of the acquired immune system, stimulating antibody production [71], while in early stages of PDAC, TGFβ has tumour suppressive effects [69]. Attending to their roles and, as we are simulating an early stage of cancer development, it makes sense for these factors to be secreted in a higher amount by healthy HDFs than in the co-cultures. Finally, the amount of TNFα secreted in the PANC-1 cultures was significantly lower than IGF-1, VEGF, FGFb, TGFβ and leptin, whilst in the co-cultures it was not significantly lower compared with the rest of the factors. In cancer tumours, TNFα has roles related with avoiding tumour proliferation and promoting tumour regression [61]. In the HDFs cultures, the secretion of TNFα was low as there is no presence of cancer cells. Therefore, we could argue that the presence of cancer cells in the co-cultures stimulated the production on TNFα and would suggest that the initial fibroblasts that arrive at the tumour site could try to fight the proliferation of tumour cells. However, TNFα has been shown to strongly influence epithelial to mesenchymal transition of human endothelial cells [62]. Therefore, it could also be argued that cancer cells stimulate fibroblasts to secrete TNFα to aid with tumour progression. Further research could clarify the role of TNFα in the early stages of PDAC development. In summary, our results suggest the complex interplay between fibroblasts and cancer cells in terms of angiogenesis in the early stages of tumour development, which seems to favour cancer cells proliferation and establishment of a vascular network to deliver oxygen and nutrients to support the high metabolic activity of the TME [75].

5. Conclusions

The novelty of this work resides in the use of EW/gelatin hydrogels for building novel cancer-on-a-chip models of PDAC. Our results demonstrate the enormous potential of using these hydrogels in these miniaturized models. Compared with other hydrogels used in cancer-on-a-chip models, our EW/gelatin hydrogels are easily available, have no ethical issues, are cost-effective, their fabrication and processing are straightforward, are highly biocompatible due to presence of molecular cues found in the ECM of tissues, and offer reproducibility of results, mechanical integrity, and effective growth of multi-cellular tumour structures. Furthermore, the importance of the microenvironment in tumour cells behaviour is clearly shown by our results and warrants further work into the 3D multi-cellular structures formed by pancreatic cancer cells in EW/gelatin hydrogels.

Funding

This work was supported by E.G-G's "Ramon & Cajal Fellowship" (RYC2021–033490-I, funded by MCIN/AEI/10.13039/501100011033 and the EU "NextGenerationEU/PRTR"). Dual-beam FIB-SEM characterization was funded by ICTS ELECMI grants ELC217–2023 and ELC384–2024. Authors would like to acknowledge the Spanish Ministry of Economy and Competitiveness (PID2020–113819RB-I00, PID2021–122409OB-C21, and PID2021–125762NB-I00) and the European Research Council (ERC) under the European Union's Horizon 2020 research and innovation programme (ICoMICS grant agreement No 101018587). KG.P and J.Z-Z gratefully acknowledge the support of Aragon Institute of Engineering Research (I3A, Ayuda para practicas con TFM) and the Spanish Ministry of Education and Professional Formation (FPU21/06003), respectively. A.C-V gratefully acknowledges the Department of Science, University, and Knowledge Society of the Government of Aragon (predoctoral contract, Call No. 2023–27).

CRediT authorship contribution statement

Karinna Georgiana Pele: Writing – review & editing, Writing – original draft, Methodology, Investigation, Formal analysis, Data curation. **Alejandro Calderón-Villalba:** Writing – review & editing, Methodology, Investigation. **Hippolyte Amaveda:** Writing – review & editing, Methodology, Investigation, Formal analysis. **Mario Mora:** Writing – review & editing, Methodology, Investigation, Formal analysis. **Jack Zhang-Zhou:** Writing – review & editing, Methodology, Investigation. **Maria Angeles Perez:** Writing – review & editing, Resources. **Jose Manuel Garcia-Aznar:** Writing – review & editing, Resources. **Pilar Alaman-Diez:** Writing – review & editing, Supervision, Methodology, Investigation, Formal analysis. **Elena Garcia-Gareta:** Writing – review & editing, Writing – original draft, Supervision, Resources, Project administration, Methodology, Investigation, Formal analysis, Data curation, Conceptualization.

Declaration of Competing Interest

The authors declare that they have no known competing financial interests or personal relationships that could have appeared to influence the work reported in this paper.

Acknowledgments

The authors acknowledge Mariano Barrado and Marta Navarro for technical support with dual-beam FIB-SEM and useful discussions, the Servicio General de Apoyo a la Investigación-SAI (University of Zaragoza) for the use of the critical point dryer, and the Laboratorio de Microscopías Avanzadas (LMA-University of Zaragoza) for the use of electron microscopes.

Appendix A. Supporting information

Supplementary data associated with this article can be found in the online version at doi:10.1016/j.colsurfb.2025.114736

Data availability

Data will be made available on request.

References

[1] A. Sontheimer-Phelps, BA Hassell, DE. Ingber, Modelling cancer in microfluidic human organs-on-chips, Nat. Rev. Cancer [Internet] 19 (2) (2019) 65–81. https://www.nature.com/articles/s41568-018-0104-6 (Available from).
[2] AG Mitrakas, A. Tsolou, S. Didaskalou, L. Karkaletsou, C. Efstathiou, E. Eftalitsidis, et al., Applications and advances of multicellular tumor spheroids: challenges in their development and analysis, Int. J. Mol. Sci. 24 (8) (2023).
[3] EC Costa, AF Moreira, D. de Melo-Diogo, VM Gaspar, MP Carvalho, IJ. Correia, 3D tumor spheroids: an overview on the tools and techniques used for their analysis, Biotechnol. Adv. 34 (8) (2016) 1427–1441.
[4] K. Han, SE Pierce, A. Li, K. Spees, GR Anderson, JA Seoane, et al., CRISPR screens in cancer spheroids identify 3D growth-specific vulnerabilities, Nat. [Internet] (2020), https://doi.org/10.1038/s41586-020-2099-x (Available from).
[5] C. Vitale, M. Marzagalli, S. Scaglione, A. Dondero, C. Bottino, R. Castriconi, Tumor microenvironment and hydrogel-based 3D cancer models for in vitro testing immunotherapies, Cancers (Basel) 14 (4) (2022) 1013.
[6] E. Prince, J. Cruickshank, W. Ba-Alawi, K. Hodgson, J. Haight, C. Tobin, et al., Biomimetic hydrogel supports initiation and growth of patient-derived breast tumor organoids, Nat. Commun. 13 (1) (2022) 1466.
[7] P. Alamán-Díez, C. Borau, P. Enrique Guerrero, H. Amaveda, M. Mora, JM Fraile, et al., Collagen-Laponite nanoclay hydrogels for tumor spheroid growth, Biomacromolecules (2023).
[8] PA Mollica, EN Booth-Creech, JA Reid, M. Zamponi, SM Sullivan, X.-L. Palmer, et al., 3D bioprinted mammary organoids and tumoroids in human mammary derived ECM hydrogels, Acta Biomater. [Internet] 95 (2019) 201–213. http://www.sciencedirect.com/science/article/pii/S1742706119304283#lt;/Elocation-id#gt; (Available from).

[9] MW Tibbitt, KS. Anseth, Hydrogels as extracellular matrix mimics for 3D cell culture, Biotechnol. Bioeng. 103 (4) (2009) 655–663.
[10] F. Redaelli, M. Sorbona, F. Rossi, Synthesis and processing of hydrogels for medical applications. In: Perale G, Hilborn J, editors. Bioresorbable Polymers for Biomedical Applications [Internet], Elsevier, 2017, pp. 205–228. https://linkinghub.Elsevier.com/retrieve/pii/B9780081002629000100 (Available from).
[11] S. Jalili-Firoozinezhad, M. Filippi, F. Mohabatpour, D. Letourneur, A. Scherberich, Chicken egg white: hatching of a new old biomaterial, Mater. Today [Internet] 40 (2020) 193–214. https://linkinghub.elsevier.com/retrieve/pii/S1369702120302170#lt;/Elocation-id#gt; (Available from).
[12] J. Alipal, NAS Mohd Pu'ad, TC Lee, NHM Nayan, N. Sahari, H. Basri, et al., A review of gelatin: Properties, sources, process, applications, and commercialisation, in: In: Materials Today: Proceedings, Elsevier Ltd., 2019, pp. 240–250.
[13] E. García-Gareta, A. Levin, L. HookEngineering the migration and attachment behaviour of primary dermal fibroblasts2019, (September 2018):1–14.
[14] J. Babaei, M. Mohammadian, A. Madadlou, Gelatin as texture modifier and porogen in egg white hydrogel, Food Chem. 270 (2019) 189–195.
[15] S. Pérez-Huertas, K. Terpiłowski, M. Tomczyńska-Mleko, K. Nishinari, S. Mleko, Surface and rheological properties of egg white albumin/gelatin dispersions gelled on cold plasma-activated glass, Food Hydrocoll. 96 (2019) 224–230.
[16] KG Pele, H. Amaveda, M. Mora, C. Marcuello, A. Lostao, P. Alamán-Díez, et al., Hydrocolloids of egg white and gelatin as a platform for hydrogel-based tissue engineering, Gels 9 (6) (2023) 505.
[17] BA Kaipparettu, I. Kuiatse, BTY Chan, MB Kaipparettu, A.V. Lee, S. Oesterreich, Novel egg white - based 3-D cell culture system, Biotech. [Internet] 45 (2) (2008) 165–171. https://www.future-science.com/doi/10.2144/000112883. Aug 16 [cited 2022 Jun 13] Available from.
[18] B. Kalyanaraman, DM Supp, ST. Boyce, Medium flow rate regulates viability and barrier function of engineered skin substitutes in perfusion culture, Tissue Eng. Part A [Internet] 14 (5) (2008) 583–593, https://doi.org/10.1089/tea.2007.0237. http://www.liebertonline.com/doi/abs/ (Available from).
[19] P. Sarantis, E. Koustas, A. Papadimitropoulou, AG Papavassiliou, M.V. Karamouzis, Pancreatic ductal adenocarcinoma: treatment hurdles, tumor microenvironment and immunotherapy Open-Access, World J. Gastrointest. Oncol. [Internet] 12 (2) (2020) 173–181. https://www.f6publishing.com (Available from).
[20] A. Bengtsson, R. Andersson, D. Ansari, The actual 5-year survivors of pancreatic ductal adenocarcinoma based on real-world data, Sci. Rep. 10 (2020) 16425.
[21] M. Miyazawa, M. Katsuda, M. Kawai, S. Hirono, K. Okada, Y. Kitahata, et al., Advances in immunotherapy for pancreatic ductal adenocarcinoma, J. Hepatobiliary Pancreat. Sci. 28 (5) (2021) 419–430.
[22] U. Vaish, T. Jain, AC Are, V. Dudeja, Cancer-associated fibroblasts in pancreatic ductal adenocarcinoma: An update on heterogeneity and therapeutic targeting. International Journal of Molecular Sciences, MDPI, 2021. Vol. 22.
[23] E. García-Gareta, A. Calderón-Villalba, P. Alamán-Díez, CG Costa, PE Guerrero, C. Mur, et al., Physico-chemical characterization of the tumour microenvironment of pancreatic ductal adenocarcinoma, Eur. J. Cell Biol. 103 (2) (2024).
[24] T. Zhang, Y. Ren, P. Yang, J. Wang, H. Zhou, Cancer-associated fibroblasts in pancreatic ductal adenocarcinoma. Cell Death and Disease, Springer Nature, 2022. Vol. 13.
[25] RH Adams, K. Alitalo, Molecular regulation of angiogenesis and lymphangiogenesis, Nat. Rev. Mol. Cell Biol. 8 (6) (2007) 464–478.
[26] Z.-L. Liu, H.-H. Chen, L.-L. Zheng, L.-P. Sun, L. Shi, Angiogenic signaling pathways and anti-angiogenic therapy for cancer, Signal Transduct. Target Ther. 8 (1) (2023) 198.
[27] V. Longo, O. Brunetti, A. Gnoni, S. Cascinu, G. Gasparini, V. Lorusso, et al., Angiogenesis in pancreatic ductal adenocarcinoma: a controversial issue, Oncotarget 7 (36) (2016) 58649–58658.
[28] M. Cóndor, T. Rüberg, C. Borau, J. Piles, JM. García-Aznar, A web-based application for automated quantification of chemical gradients induced in microfluidic devices, Comput. Biol. Med [Internet] 95 (2018) 118–128. https://linkinghub.elsevier.com/retrieve/pii/S0010482518300234#lt;/Elocation-id#gt; (Available from).
[29] S. Hernández-Hatibi, PE Guerrero, JM García-Aznar, E. García-Gareta, Polydopamine interfacial coating for stable tumor-on-a-chip models: application for pancreatic ductal adenocarcinoma, Biomacromolecules 25 (8) (2024) 5169–5180.
[30] N. Walter, A. Micoulet, T. Seufferlein, JP. Spatz, Direct assessment of living cell mechanical responses during deformation inside microchannel restrictions, Biointerphases [Internet] 6 (3) (2011) 117–125. https://pubs.aip.org/avs/bip/article/6/3/117-125/133760 (Available from).
[31] C. Helary, I. Bataille, A. Abed, C. Illoul, A. Anglo, L. Louedec, et al., Concentrated collagen hydrogels as dermal substitutes, Biomater. [Internet] 31 (3) (2010) 481–490, https://doi.org/10.1016/j.biomaterials.2009.09.073 (Available from dx.doi.org/).
[32] SC Ramaiahgari, MW den Braver, B. Herpers, V. Terpstra, JNM Commandeur, B. van de Water, et al., A 3D in vitro model of differentiated HepG2 cell spheroids with improved liver-like properties for repeated dose high-throughput toxicity studies, Arch. Toxicol. (2014).
[33] K. Shiga, M. Hara, T. Nagasaki, T. Sato, H. Takahashi, H. Takeyama, Cancer-associated fibroblasts: their characteristics and their roles in tumor growth, Cancers (Basel) 7 (4) (2015) 2443–2458.
[34] I. Marech, C. Leporini, M. Ammendola, M. Porcelli, CD Gadaleta, E. Russo, et al., Classical and non-classical proangiogenic factors as a target of antiangiogenic therapy in tumor microenvironment, Cancer Lett. 380 (1) (2016) 216–226.
[35] S. Nour, R. Imani, AM. Sharifi, Angiogenic effect of a nanoniosomal deferoxamine-loaded poly(vinyl alcohol)-egg white film as a promising wound dressing, ACS Biomater. Sci. Eng. 8 (8) (2022) 3485–3497.
[36] NZ Renkler, E. Ergene, S. Gokyer, M. Tuzlakoglu Ozturk, P. Yilgor Huri, K. Tuzlakoglu, Facile modification of polycaprolactone nanofibers with egg white protein, J. Mater. Sci. Mater. Med 32 (4) (2021).
[37] DJ Patty, AD Nugraheni, ID Ana, Y. Yusuf, Dual functional carbonate-hydroxyapatite nanocomposite from Pinctada maxima and egg-white for bone tissue engineering, J. Biomater. Sci. Polym. Ed. [Internet] 33 (8) (2022) 1043–1062, https://doi.org/10.1080/09205063.2022.2036934 (Available from).
[38] NT Carpena, CDG Abueva, AR Padalhin, B.-T. Lee, Evaluation of egg white ovomucin-based porous scaffold as an implantable biomaterial for tissue engineering, J. Biomed. Mater. Res Part B Appl. Biomater. [Internet] 105 (7) (2017) 2107–2117, https://doi.org/10.1002/jbm.b.33750 (Available from).
[39] Y. Mousseau, S. Mollard, H. Qiu, L. Richard, R. Cazal, A. Nizou, et al., In vitro 3D angiogenesis assay in egg white matrix: comparison to Matrigel, compatibility to various species, and suitability for drug testing, Lab Invest. 94 (3) (2014) 340–349.
[40] Z. Guo, T. Zhang, X. Chen, K. Fang, M. Hou, N. Gu, The effects of porosity and stiffness of genipin cross-linked egg white simulating aged extracellular matrix on proliferation and aggregation of ovarian cancer cells, Colloids Surf. A Physicochem Eng. Asp. 520 (2017) 649–660.
[41] J. Plou, Y. Juste-Lanas, V. Olivares, C. del Amo, C. Borau, JM. García-Aznar, From individual to collective 3D cancer dissemination: roles of collagen concentration and TGF-β, Sci. Rep. [Internet] 8 (1) (2018) 12723. http://www.nature.com/articles/s41598-018-30683-4 (Available from).
[42] SV Nolte, W. Xu, H.-O. Rennekampff, HP. Rodemann, Diversity of fibroblasts – a review on implications for skin tissue engineering, Cells Tissues Organs [Internet] 187 (3) (2008) 165–176, https://doi.org/10.1159/000111805. https://karger.com/CTO/article/doi/ (Available from).
[43] CP Huang, J. Lu, H. Seon, AP Lee, LA Flanagan, H.-Y. Kim, et al., Engineering microscale cellular niches for three-dimensional multicellular co-cultures, Lab Chip 9 (12) (2009) 1740.
[44] S. Park, T. Kim, S. Kim, S. You, Y. Jung, Three-dimensional vascularized lung cancer-on-a-chip with lung extracellular matrix hydrogels for in vitro screening, Cancers (Basel) 13 (16) (2021) 3930.
[45] CF Monteiro, IA Deus, IB Silva, IF Duarte, CA Custódio, JF. Mano, Tumor-on-a-chip model incorporating human-based hydrogels for easy assessment of metastatic tumor inter-heterogeneity, Adv. Funct. Mater. 34 (30) (2024).
[46] Y. Fan, DT Nguyen, Y. Akay, F. Xu, M. Akay, Engineering a brain cancer chip for high-throughput drug screening, Sci. Rep. 6 (1) (2016) 25062.
[47] EA Aisenbrey, WL. Murphy, Synthetic alternatives to Matrigel, Nat. Rev. Mater. 5 (7) (2020) 539–551.
[48] J. Clauzel, N. Colitti, M. Combeau, W. Labriji, L. Robert, A. Brilhault, et al., In vivo biocompatibility assessment of 3D printed bioresorbable polymers for brain tissue regeneration. A feasibility study, Regen. Ther. 26 (2024) 941–955.
[49] E. García-Gareta, MÁ Pérez, JM. García-Aznar, Decellularization of tumours: A new frontier in tissue engineering. Journal of Tissue Engineering, SAGE Publications Ltd., 2022. Vol. 13.
[50] T. Croguennec, F. Nau, G. Brulé, Influence of pH and Salts on Egg White Gelation, J. Food Sci. [Internet] 67 (2) (2002) 608–614. https://onlinelibrary.wiley.com/doi/full/10.1111/j.1365-2621.2002.tb10646.x. Mar 1 [cited 2022 Jun 13] Available from.
[51] A. Hayashi, S.-C. Oh, Gelation of gelatin solution, Agric. Biol. Chem. 47 (8) (1983) 1711–1716.
[52] L. Bozec, M. Odlyha, Thermal denaturation studies of collagen by microthermal analysis and atomic force microscopy, Biophys. J. 101 (1) (2011) 228–236.
[53] KM Pawelec, SM Best, RE. Cameron, Collagen: a network for regenerative medicine, J. Mater. Chem. B 4 (40) (2016) 6484–6496.
[54] AJ Holder, N. Badiei, K. Hawkins, C. Wright, PR Williams, DJ. Curtis, Control of collagen gel mechanical properties through manipulation of gelation conditions near the sol–gel transition, Soft Matter 14 (4) (2018) 574–580.
[55] M. Sheth, M. Sharma, M. Lehn, H. Reza, T. Takebe, V. Takiar, et al., Three-dimensional matrix stiffness modulates mechanosensitive and phenotypic alterations in oral squamous cell carcinoma spheroids, APL Bioeng. 8 (3) (2024).
[56] X. Di, X. Gao, L. Peng, J. Ai, X. Jin, S. Qi, et al., Cellular mechanotransduction in health and diseases: from molecular mechanism to therapeutic targets, Signal Transduct. Target Ther. 8 (1) (2023) 282.
[57] F. Zanconato, M. Cordenonsi, S. Piccolo, YAP/TAZ at the Roots of Cancer, Cancer Cell 29 (6) (2016) 783–803.
[58] TL Dayton, N. Alcala, L. Moonen, L. den Hartigh, V. Geurts, L. Mangiante, et al., Druggable growth dependencies and tumor evolution analysis in patient-derived organoids of neuroendocrine neoplasms from multiple body sites, Cancer Cell 41 (12) (2023) 2083–2099.e9.
[59] Y. Li, L. Zhao, X.-F. Li, Hypoxia and the Tumor Microenvironment, Technol. Cancer Res Treat. 20 (2021), 153303382110363.
[60] G. Bergers, LE. Benjamin, Tumorigenesis and the angiogenic switch, Nat. Rev. Cancer 3 (6) (2003) 401–410.
[61] X. Wang, Y. Lin, Tumor necrosis factor and cancer, buddies or foes? Acta Pharm. Sin. 29 (11) (2008) 1275–1288.
[62] M. Adjuto-Saccone, P. Soubeyran, J. Garcia, S. Audebert, L. Camoin, M. Rubis, et al., TNF-α induces endothelial–mesenchymal transition promoting stromal development of pancreatic adenocarcinoma, Cell Death Dis. 12 (7) (2021) 649.
[63] T. Shanmugalingam, C. Bosco, AJ Ridley, M. Van Hemelrijck, Is there a role for IGF-1 in the development of second primary cancers? Cancer Med 5 (11) (2016) 3353–3367.

[64] A. Ardizzone, V. Bova, G. Casili, A. Repici, M. Lanza, R. Giuffrida, et al., Role of Basic Fibroblast Growth Factor in Cancer: Biological Activity, Targeted Therapies, and Prognostic Value, Cells 12 (7) (2023) 1002.
[65] Y. Fan, Y. Gan, Y. Shen, X. Cai, Y. Song, F. Zhao, et al., Leptin signaling enhances cell invasion and promotes the metastasis of human pancreatic cancer via increasing MMP-13 production, Oncotarget 6 (18) (2015) 16120–16134.
[66] J. Park, PE Scherer, Leptin and cancer: from cancer stem cells to metastasis, Endocr. Relat. Cancer 18 (4) (2011) C25–C29.
[67] P. Carmeliet, VEGF as a key mediator of angiogenesis in cancer, Oncology 69 (3) (2005) 4–10.
[68] Z. Zhang, S. Ji, B. Zhang, J. Liu, Y. Qin, J. Xu, et al., Role of angiogenesis in pancreatic cancer biology and therapy, Biomed. Pharm. 108 (2018) 1135–1140.
[69] V. Syed, TGF-β Signaling in Cancer, J. Cell Biochem 117 (6) (2016) 1279–1287.
[70] Q. Luo, Z. Hu, H. Zhao, Y. Fan, X. Tu, Y. Wang, et al., The role of TGF-β in the tumor microenvironment of pancreatic cancer, Genes Dis. 10 (4) (2023) 1513–1524.
[71] T. Tanaka, M. Narazaki, T. Kishimoto, IL-6 in inflammation, immunity, and disease, Cold Spring Harb. Perspect. Biol. 6 (10) (2014) a016295, a016295.
[72] J. Chen, Y. Wei, W. Yang, Q. Huang, Y. Chen, K. Zeng, et al., IL-6: the link between inflammation, immunity and breast cancer, Front Oncol. 12 (2022).
[73] G. van Duijneveldt, MDW Griffin, TL. Putoczki, Emerging roles for the IL-6 family of cytokines in pancreatic cancer, Clin. Sci. 134 (16) (2020) 2091–2115.
[74] S. Sigismund, D. Avanzato, L. Lanzetti, Emerging functions of the <scp>EGFR< / scp> in cancer, Mol. Oncol. 12 (1) (2018) 3–20.
[75] R. Kalluri, M. Zeisberg, Fibroblasts in cancer, Nat. Rev. Cancer 6 (5) (2006) 392–401.